Strain Engineering of Single-Layer MoS_2

Manouchehr Hosseini*, Mohammad Elahi*, Ebrahim Asl Soleimani*, Mahdi Pourfath*†, and David Esseni‡

*School of Electrical and Computer Engineering, University of Tehran, Iran

† Institute of Microelectronics, TU Wien, Gusshausstrasse 27-29/E360, 1040 Vienna, Austria

Email: pourfath@ut.ac.ir & pourfath@iue.tuwien.ac.at

‡DIEGM, Via delle Scienze 206, 33100 Udine, Italy

Email: david.esseni@uniud.it

***Abstract*—In this work the effect of biaxial and uniaxial strain on the mobility of single-layer MoS_2 at room temperatures is comprehensively studied. Scattering from intrinsic phonon modes, remote phonon and charged impurities are considered along with static screening. Ab-initio simulations are utilized to investigate the strain induced effects on the electronic bandstructure and the linearized Boltzmann transport equation is used to evaluate the low-field mobility under various strain conditions. The results indicate that the mobility increases with tensile biaxial and tensile uniaxial strain along the armchair direction. Under compressive strain, however, the mobility exhibits a non-monotonic behavior when the strain magnitude is varied. In particular, with a relatively small compressive strain of 1% the mobility is reduced by about a factor of two compared to the unstrained condition, but with a larger compressive strain the mobility partly recovers such a degradation.**

I. Introduction

Single and few-layers of transition metal dichalcogenides show promising electronic, optical, and mechanical properties and are considered as potential candidates for future electronic applications [1]. Because of weak interlayer van der Waals bonds in their layered structure, single to few-layers of these materials can be obtained by mechanical or chemical exfoliation techniques [2], [3]. Among these materials single-layer MoS_2 has attracted the attention of scientists and many studies have been performed on characterizing the properties of this material [4], [5]. Single-layer MoS_2 has a direct band gap of 1.8 eV [5], which makes it suitable for various electronic applications. An MOS transistor based on this material has demonstrated a I_{on}/I_{off} ratio of 10^8, a relatively steep subthreshold swing of 74 mV/dec and an extremely small off-current of 25 fA/μm [6] and possible applications to hetero-junction interlayer tunneling FETs have also been proposed and theoretically investigated. [7] Room temperature mobility of n-type single-layer MoS_2 is reported to be in the range of 0.5–3 cm^2/(Vs) and can be increased to about 200 cm^2/(Vs) with the use of high-κ dielectrics. [6] However, a comprehensive study of strain effects on the mobility of this material is missing.

II. Approach

We carry out first-principle simulations based on the density-functional theory (DFT) along with the local density approximation (LDA) as implemented in the SIESTA code [8] to investigate the relevant electronic properties of a single layer MoS_2 under strain. A cutoff energy equal to 600 Ry is used and a vacuum separation of 30 Å is adopted, which is sufficient to hinder interactions between adjacent layers. Sampling of the reciprocal space Brillouin zone (BZ) is performed by a Monkhorst-Pack grid of $18 \times 18 \times 1$ k-points. Calculations begin with the determination of the optimized geometry, that is the configuration in which the residual Hellmann-Feynman forces acting on atoms are smaller than 0.01 eV/Å. The calculated lattice constant of unstrained single-layer MoS_2 is 3.11 Å. Fig. 1 shows the energy contours of the conduction-band in the first BZ with and without strain. In an unstrained material the lowest and the second lowest minimum in the conduction

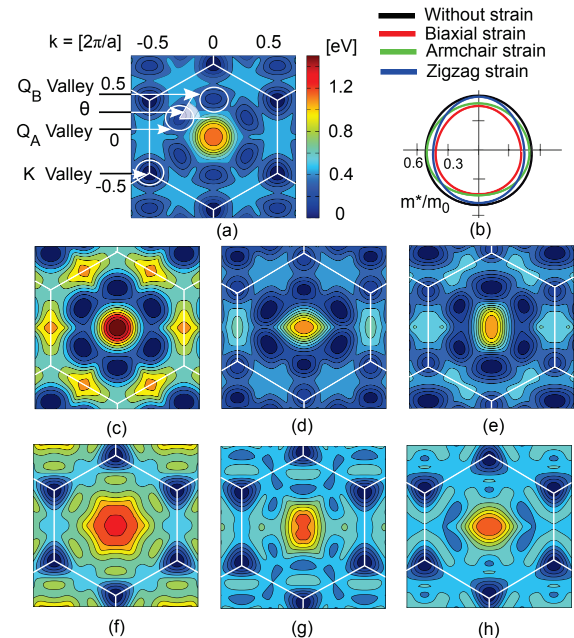

Fig. 1. (a) The energy contours in the first Brillouin zone for unstrained single layer MoS_2. The k-space representation of the angle associated with the Q_A valley is also depicted in this figure (the zigzag direction in k-space is the dual of the armchair direction in real space). (b) Extracted effective mass of K-valley along all directions in polar coordinate for unstrained MoS_2 and under tensile biaxial and uniaxial strain along armchair and zigzag directions. The nearly circular shape of the effective mass plot, justifies the assumption of isotropic band-structure. The energy contours for single layer MoS_2 under: (c) compressive biaxial strain; (d) compressive uniaxial strain along the zigzag direction; (e) compressive uniaxial strain along the armchair direction; (f) tensile biaxial strain; (g) tensile uniaxial strain along the zigzag direction and (h) tensile uniaxial strain along the armchair direction. The strain magnitude is 4% in all strained cases. The longitudinal and transverse effective masses of Q-valleys vary with the strain conditions.

978-1-4673-7135-3/15/$31.00 ©2015 IEEE

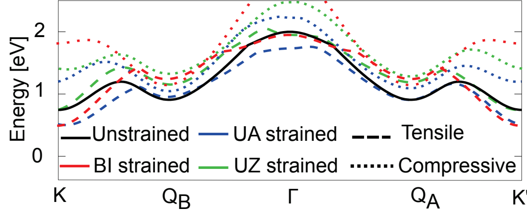

Fig. 2. The conduction band of unstrained and strained single layer MoS_2. BI: biaxial strain, UA: uniaxial strain along armchair direction; UZ: uniaxial strain along zigzag direction. The strain magnitude is 4% in all strained cases.

band are denoted as K-valley and Q-valley, respectively. The energy distance between these valleys for unstrained material is evaluated to be 160 meV, in agreement with Ref. [9]. The 6 Q-valleys are degenerate for unstrained and biaxial strain conditions. With the application of uniaxial strain, however, they split into 4 Q_A-valleys and 2 Q_B-valleys with different effective masses and energy minima.

To evaluate the low-field mobility we solved the linearized Boltzmann equation (BTE), employing the method described in Ref. [11]. In order to describe in more detail the mobility calculation procedure, we first recall that the longitudinal direction of Q_A-valley is neither the armchair nor the zigzag direction, and Fig. 1(a) shows that θ is the angle describing the valley orientation with respect to the zigzag direction in k-space (i.e. armchair direction in real space). Let us now consider first the case of the mobility $\mu_A^{(v)}$ of valley v along the armchair direction, that can be written by definition as $\mu_A^{(v)} = J_A^{(v)}/F_A$, where $J_A^{(v)}$ is the current component in the armchair direction for the valley v induced by the electric field F_A along armchair direction. The current $J_A^{(v)}$ can be expressed as $J_A^{(v)} = J_l^{(v)} \cos(\theta_v) + J_t^{(v)} \sin(\theta_v)$ in terms of the current components $J_l^{(v)}$, $J_t^{(v)}$ along, respectively, the longitudinal and transverse direction of the valley v. By denoting the longitudinal (F_l) and transverse component (F_t) of the electric field as $F_l = F_A cos(\theta_v)$ and $F_t = F_A \sin(\theta_v)$, the currents $J_l^{(v)}$ and $J_t^{(v)}$ in turn can be written as $J_l^{(v)} = \mu_{ll}^{(v)} F_l + \mu_{lt}^{(v)} F_t$ and $J_t^{(v)} = \mu_{lt}^{(v)} F_l + \mu_{tt}^{(v)} F_t$, where μ_{ll}, μ_{tt} and μ_{lt} are the entries of the two by two mobility matrix in the valley coordinate system . For the circular and elliptical bands employed in our calculations, μ_{tl} and μ_{lt} are zero for symmetry reasons [12]. Consequently we finally obtain:

$$\mu_A^{(v)} = \mu_{ll}^{(v)} \cos^2(\theta_v) + \mu_{tt}^{(v)} \sin^2(\theta_v) \ , \tag{1}$$

By following a similar procedure, the mobility $\mu_Z^{(v)}$ of the valley v along the zigzag direction can be written as:

$$\mu_Z^{(v)} = \mu_{ll}^{(v)} \sin^2(\theta_v) + \mu_{tt}^{(v)} \cos^2(\theta_v) \ , \tag{2}$$

After calculating the mobility for each valley, the overall mobility is obtained as the average of the mobility in the different valleys weighted by the the corresponding electron density.

Scattering rates due to intrinsic phonons (including acoustic, optical and polar-optical phonons), to remote phonons and to charged impurities are taken into account. Piezoelectric coupling to the acoustic phonons is only important at low temperatures and is neglected in this work. The phonon assisted inter-valley transitions considered in this work. In our calculations, we employed the deformation potentials and phonon energies from Ref. [13]. It should be noted that the same deformation potentials are used for Q_A and Q_B valleys. Another important source of scattering considered in this work is the remote phonon or surface-optical (SO) phonon scattering mechanism. We calculate the effect of SO phonon by assuming semi-infinite oxides and neglecting the possible coupling to the plasmons of the two-dimensional material [14]. To investigate the effect of the dielectric environment on the scattering of carriers from charged impurities located inside the single layer MoS_2, we assume that the charged impurities are located in the center of the single layer MoS_2 thickness [12].

The effect of static screening on charged impurities is included by using the dielectric function approach [12]. For the inelastic, intervalley phonon transitions described the relatively large phonon wave-vector) and the non-null phonon energies suggest that it is safe to leave these transitions unscreened, because the dynamic descreening and the large phonon wave-vectors make the screening very ineffective. Arguments concerning screening for intra-valley acoustic phonons are more subtle and controversial and a thorough discussion for inversion layer systems can be found in Ref. [15]. We here decided to leave also intra-valley acoustic phonons unscreened, which is the choice employed in essentially all the studies concerning transport in inversion layers that the authors are aware of. The screening of the SO phonon scattering is also a delicate subject, because the polar phonon modes of the high-κ dielectrics can couple with the collective excitations of the electrons in the MoS_2 layer and thus produce coupled phonon-plasmon modes [14], [15], whose treatment is further complicated by the possible occurrence of Landau damping [14]–[16]. In this paper we do not attempt a full treatment of the coupled phonon-plasmon modes [14], [15], but instead show results for the two extreme cases of either unscreened SO phonons or SO phonons screened according to the static dielectric function. We can anticipate that while the inclusion of static screening in SO phonons implies a significant mobility enhancement compared to the unscreened case, the mobility dependence on the strain and on the dielectric constant of the high-κ dielectrics is not significantly affected by the treatment of screening for SO phonons [12].

III. Results and Discussions

Fig. 2 illustrates the conduction band of unstrained and strained single layer MoS_2 including K, Q_A, and Q_B valleys. Under compressive strain one of the Q_A or Q_B valleys becomes the lowest valley. The energy distance between these K-valley and Q-valley for unstrained material is evaluated to be 160 meV, in agreement with Ref. [9]. Tensile strain increases this energy distance, which is instead reduced by a compressive strain. In particularly, a relatively large compressive strain lowers the energy of Q-valley so that it becomes the lowest val-

TABLE I
COMPARISON OF THE CALCULATED MOBILITY IN THIS WORK WITH THE EXPERIMENTAL DATA OF REF. [10].

Carrier concentration cm^{-2}	7.6×10^{12}	9.6×10^{12}	1.15×10^{13}	1.35×10^{13}
Calculated mobility, this work [cm^2/(Vs)]	93	106	114	122
Experimental mobility [cm^2/(Vs)]	96±3	111±3	128±3	132±3

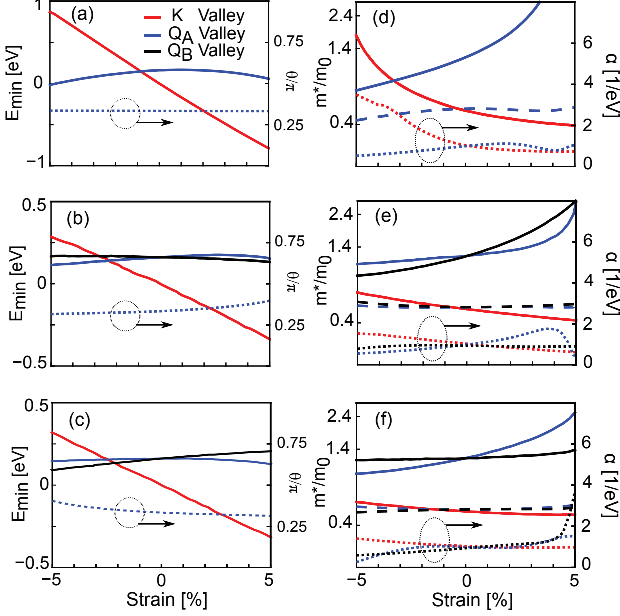

Fig. 3. The minimum energies of valleys (solid-lines) and the angle θ (dotted lines) between the longitudinal direction of Q_A valleys and zigzag direction in k-space as illustrated in Fig. 1(a) under: (a) biaxial strain; (b) uniaxial strain along the armchair direction; (c) uniaxial strain along the zigzag direction. The θ angle in Fig. 3(a)-(c) corresponds to the Q_A valley indicated in Fig. 1(a), and the θ angle of the other Q_A valleys can be inferred from symmetry considerations. The θ angle for Q_B valleys has a negligible dependence on strain (not shown) and it is approximately zero (see Fig. 1(a)). The effective masses (solid-lines for longitudinal and dashed-lines for transverse) and the non-parabolicity factor (α) (dotted-lines) of various valleys under: (d) biaxial strain; (e) uniaxial strain along the armchair direction; (f) uniaxial strain along the zigzag direction. The longitudinal and transverse effective masses of K-valley are assumed to be equal.

ley as shown in Fig. 3(a)-(c). Here we can anticipate that, while under tensile strain one can neglect the scattering between Q and K-valleys, under compressive strain this type of scattering can significantly affect the mobility. Assuming a non-parabolic dispersion relation $E(1+\alpha E) = \hbar^2 k_l^2/2m_l^* + \hbar^2 k_t^2/2m_t^*$, the longitudinal m_l^* and transverse m_t^* effective mass and also the non-parabolicity factor α are extracted from the DFT-calculated electronic bandstructure and reported in Fig. 3(d)-(f). As can be seen in Fig. 3(a)-(c), under compressive uniaxial strain the energy minima of all K- and Q-valleys are quite close, while at large compressive biaxial strain the K-valley lie at higher energy and their contribution to mobility can be neglected.

We compare in Table I our calculated mobilities at various carrier concentrations with the experimental data reported in Ref. [10] for unstrained single-layer MoS_2 embedded between SiO_2 and HfO_2 with impirity density 4 $\times 10^{12}$ and at $T = 100$ K, where the effect of piezoelectric can be ignored [17]. Very good agreement with experimental data validates the bandstructure and mobility models employed in this work.

The strain-dependency of intrinsic phonon limited mobility is presented in Fig. 4(a). Apparently, the effects of compressive and tensile strain on mobility are very different, which can be mainly explained by considering the role of inter-valley scattering. For example, with tensile strain the minimum energies of Q_A and Q_B-valleys are much higher than that of K-valley, which suppresses inter-valley scattering. Under compressive strain, instead, the inter-valley scattering cannot be neglected because of the smaller energy difference between these valleys. With tensile biaxial strain, the mobility increases because of the reduction of the effective mass and also the increase of the energy difference between K and Q-valleys, which results in the reduction of the inter-valley scattering rate. With a tensile biaxial strain of 5% the phonon limited mobility becomes 75% higher than that of unstrained material. In contrast, a compressive biaxial strain of 0.8% strongly reduces the mobility due to the reduction of energy difference between K and Q-valleys (see Fig. 3(a)) and increased inter-valley scattering. With further increase of compressive biaxial strain, Q-valleys become the lowest ones and thus dominate the mobility. At a strain value of about 2.5% the contribution of K-valleys to mobility becomes negligible and the mobility behavior is completely determined by the Q-valleys. Longitudinal and transverse effective masses of Q-valleys are not equal and are somewhat changed by strain, however, the different angular dependency of mobility along the armchair and zigzag direction tends to compensate the changes of effective masses and the overall mobility remains nearly constant at larger compressive strain values.

Under tensile uniaxial strain the mobility is hardly affected by a strain along the zigzag direction, while it increases for strain along the armchair direction. In both cases the variation of the effective mass and non-parabolicity factor with strain determine the mobility behavior. Under a compressive uniaxial strain along the armchair direction, Q_A becomes the lowest valley, while for a strain along the zigzag direction Q_B is the lowest one. These results emphasize that the contribution of both Q_A and Q_B valley should be included for an accurate calculation of mobility. Under a compressive strain of about 1.5% the mobilities are strongly reduced, but they remain nearly constant for larger strain magnitudes. Moreover, we notice that for a strain along the zigzag direction, the mobility along the strain direction becomes slightly larger than the mobility in the armchair direction.

Fig. 4(b) reports the mobility in the presence of intrinsic phonon and charged impurity scattering. The top and bottom

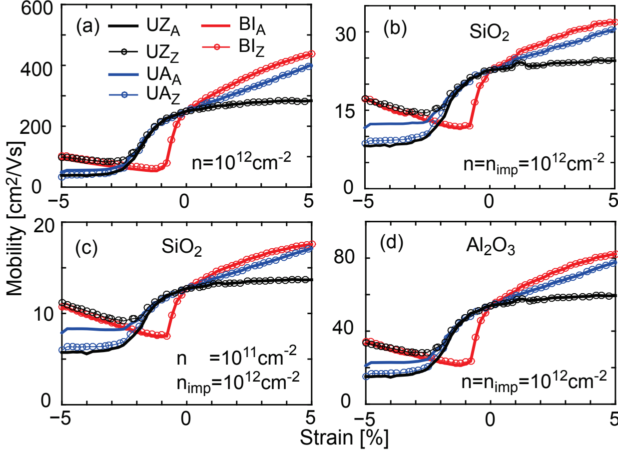

Fig. 4. (a) Phonon limited mobility of single layer MoS_2 as a function of strain with a carrier concentration $n = 10^{12}$ cm^{-2}. Mobility limited by phonon and screened charged impurity scattering with SiO_2 as the gate oxide (ϵ_r = 3.9) and carrier (n) and charged impurity concentration (n_{imp}) for: (b) $n = n_{\text{imp}} = 10^{12}$ cm^{-2}; (c) $n = 10^{11}$ cm^{-2} and $n_{\text{imp}} = 10^{12}$ cm^{-2}. (d) Same as (b), except for the gate oxide which is Al_2O_3. In the legend, BI, UA, and UZ denote biaxial strain, uniaxial strain along the armchair direction, and uniaxial strain along the zigzag direction respectively. The subscripts A and Z indicate the component of the mobility along the armchair or zigzag direction. For example: UZ_A is the mobility along armchair direction for a uniaxial strain along zigzag direction.

oxide are assumed to be SiO_2 and both carrier and impurity concentrations are 10^{12} cm^{-2}. Except for a global reduction of the mobility, the behavior of the mobility with strain is similar to Fig. 4(a) corresponding to phonon limited mobility. The results presented in Fig. 4(c) correspond to the same parameters as in Fig. 4(b), except for a reduction of carrier concentration to 10^{11} cm^{-2}. As the carrier concentration decreases the effect of static screening becomes weaker and the mobility is further reduced. Fig. 4(d) illustrates the mobility as a function of strain with the same parameters used in Fig. 4(b), expect for the top and bottom gate oxide which is Al_2O_3. A high-κ dielectric implies a larger dielectric screening and increases the mobility. Under this condition, with a tensile biaxial strain of 5% and a tensile uniaxial strain of 5% along the armchair direction the mobility increases by 53% and 43%, respectively, compared to an unstrained single-layer MoS_2.

The effect of unscreened and screened remote phonon scattering on the mobility of unstrained and 5% biaxial strained single layer MoS_2 are compared in Fig. 5. Except for a global increase of mobility values. The mobility dependence on the dielectric constant κ is not significantly affected by the screening of SO phonons. As can be seen, for relatively small κ values, mobility improves with increasing κ because of the dielectric screening of charged impurities [18]. At high κ values, however, the mobility decrease with increasing κ because the corresponding smaller SO phonon energies tend to increase momentum relaxation time via SO phonons. For the conditions considered in Fig. 5(temperature, carrier and impurity concentrations, and semi-infinite dielectrics with SiO_2 as the bottom oxide), AlN appears to be the optimal top dielectric material.

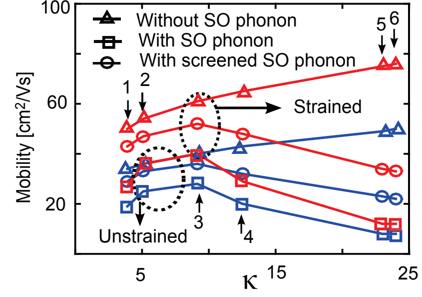

Fig. 5. The mobility accounting for intrinsic phonon and charged impurity scattering (triangle), and for either unscreened (rectangle) or screened (circle) SO phonon scattering as a function of top oxide dielectric constant for unstrained (blue line) and 5% biaxial strain (red line). Numbers 1 to 6 indicate the κ value corresponding to dielectric materials studied in this work. In particular, (1): SiO_2, (2): BN, (3): AlN, (4): Al_2O_3, (5): HfO_2, and (6): ZrO_2. In all cases the back oxide is assumed to be SiO_2. T = 300 K, the impurity and carrier concentrations are equal to 4×10^{12} cm^{-2} and 10^{13} cm^{-2}, respectively. These values are consistent with experimental data reported in Ref. [10].

IV. Conclusion

A comprehensive theoretical study on the role of strain on the mobility of single-layer MoS_2 is presented. DFT calculations are used to obtain the effective masses and minima of the contributing valleys. Thereafter, the linearized BTE is solved for evaluating the mobility, including the effect of phonon and screened charged impurities. The results indicate that, a tensile strain increase the mobility, while compressive strain reduces mobility. Furthermore, biaxial strain and uniaxial strain along the armchair direction increase the mobility more effectively. The strain-dependency of the mobility of MoS_2 is rather complicated and strongly depends on the relative positions of Q and K-valleys and the corresponding inter-valley scattering. The presented results pave the way for a possible strain engineering of the electronic transport in MoS_2 based electron devices.

Acknowledgement

This work was partly supported by the Iran National Science Foundation (INSF).

References

[1] A. Neto *et al.*, Rep. Prog. Phys. **74**, 82501 (2011).
[2] K. Novoselov *et al.*, Proc. Nat. Acad. Sci. **102**, 10451 (2005).
[3] H. Ramakrishna Matte *et al.*, Angew. Chem. Int. Ed. **122**, 4153 (2010).
[4] A. Splendiani *et al.*, Nano Lett. **10**, 1271 (2010).
[5] K. F. Mak *et al.*, Phys. Rev. Lett. **105**, 136805 (2010).
[6] B. Radisavljevic *et al.*, Nature Nanotech. **6**, 147 (2011).
[7] M. O. Li *et al.*, J. Appl. Phys. **115**, 074508 (2014).
[8] J. M. Soler *et al.*, J. Phys.: Condens. Matter **14**, 2745 (2002).
[9] K. Kaasbjerg *et al.*, Phys. Rev. B **85**, 115317 (2012).
[10] B. Radisavljevic *et al.*, Nature Mater. **12**, 815 (2013).
[11] A. Paussa *et al.*, J. Appl. Phys. **113**, 093702 (2013).
[12] D. Esseni *et al.*, *Nanoscale MOS Transistors* (Cambridge University Press, Cambridge, 2011).
[13] X. Li *et al.*, Phys. Rev. B **87**, 115418 (2013).
[14] Z.-Y. Ong *et al.*, Phys. Rev. B **88**, 045405 (2013).
[15] M. V. Fischetti *et al.*, Phys. Rev. B **48**, 2244 (1993).
[16] P. Toniutti *et al.*, J. Appl. Phys. **112**, 034502 (2012).
[17] K. Kaasbjerg *et al.*, Phys. Rev. B **87**, 235312 (2013).
[18] N. Ma *et al.*, Phys. Rev. X **4**, 011043 (2014).